

Noncontact thermal characterization of multiwall carbon nanotubes

Xinwei Wang,^{a)} Zhanrong Zhong, and Jun Xu

Department of Mechanical Engineering, N104 Walter Scott Engineering Center, The University of Nebraska-Lincoln, Lincoln, Nebraska 68588-0656

(Received 1 June 2004; accepted 3 December 2004; published online 1 March 2005)

In this work, a photothermal experiment is designed and conducted to characterize the thermal transport in carbon nanotubes (CNTs) along the axial direction exclusively. We characterize the thermal contact resistance between CNTs and the substrate. The measured value demonstrates a sound thermal contact between them. Our experimental result reveals a low thermal conductivity of the CNTs along their axial direction. The unique structure of the CNTs characterized in our work indicates that the thermal transport in the axial direction is across the carbon atomic layers. This explains why the measured thermal conductivity is much lower than theoretical predictions, in which the thermal conductivity is along the atomic layer direction. In addition, our transmission electron microscope observation of the CNTs reveals poor structural qualities, which can strongly enhance phonon scattering and reduce the thermal conductivity. © 2005 American Institute of Physics. [DOI: 10.1063/1.1854725]

I. INTRODUCTION

The unique structure and dimension of carbon nanotubes (CNTs) lead to physical properties that have prompted a wide variety of potential applications. Knowledge of thermal transport in CNTs in these engineering applications is crucial for achieving desired device functions, optimizing system performance, and improving the dependability of devices. In recent years, a number of theoretical and experimental studies have been undertaken to investigate the thermophysical properties of nanowires/tubes with great emphasis placed on CNTs. An extensive review of phonons in CNTs has been conducted by Dresselhaus and Eklund,¹ in which studies on thermal properties of CNTs have been discussed. For theoretical investigations of heat transfer in CNTs, the obtained data for the thermal conductivity has shown great deviations. Using molecular dynamics (MD) simulation, Berber, Kwon, and Tománek² reported a room temperature thermal conductivity of 6600 W/m K for (10, 10) single-wall CNTs (SWCNTs), while a much different value of 1600 W/m K was proposed by Osman and Srivastava.³ Applying the theory of force field, Che, Çağın, and Goddard pointed out that the thermal conductivity of (10, 10) SWCNTs was 2980 W/m K, differing much from the above results. Maruyama⁵ performed nonequilibrium MD simulation and found that the thermal conductivity of SWCNTs increased linearly with their length up to 0.5 μm . In his work, the thermal conductivity of a (10, 10) SWCNT 200 nm long was calculated to be ~ 375 W/m K at room temperature.

As for the experimental study, only a handful of experiments have been conducted to measure the thermal conductivity of CNTs. Hone *et al.*⁶ measured the thermal conductivity of dense-packed SWCNT ropes, and attained a value of 35 W/m K for an as-grown mat sample and only 2.3 W/m K for the sintered sample. It is worth noting that

these experimental results differ significantly from the theoretical predictions (1600–6600 W/m K).^{2–4} Later, the thermal conductivity of parallel SWCNTs was measured,^{7,8} and a larger value of 218 W/m K was obtained, which was still much smaller than the theoretical predictions reviewed above. The thermal conductivity of C₆₀-filled SWCNTs was measured to be ~ 15 W/m K using the comparative method.⁹ Recently, Shi *et al.*¹⁰ measured the thermal and thermoelectric properties of one-dimensional nanostructures using a microfabricated device. They reported thermal conductivities of ~ 3 W/m K and 150 W/m K for SWCNT bundles of 148 and 10 nm diameters, respectively.

For multiwall CNTs, experiments conducted by Yi *et al.*,¹¹ Xie *et al.*,¹² and Lu, Yi, and Zhang¹³ led to a thermal conductivity of only about 27 W/m K. For an aligned multiwall CNT array, Borca-Tasciuc *et al.*¹⁴ reported anisotropic thermal diffusivities that were two orders of magnitude smaller than that anticipated from individual CNTs. Yang *et al.*¹⁵ measured the thermal conductivity of aligned multiwall CNT arrays to be 12–17 W/m K. They estimated the thermal conductivity of pure nanotubes to be ~ 200 W/m K. Kim *et al.*¹⁶ measured the thermal conductivity of an individual CNT to be over 3000 W/m K at room temperature. They estimated the mean free path of phonons in the nanotube to be around 500 nm, comparable to the effective length of the tube (2.5 μm). Therefore, the boundary scattering of phonons could substantially reduce the measured thermal conductivity. The techniques employed in these experimental studies involved bonding samples and sensors/heaters together. As a result, an appreciable thermal contact resistance between the sample and heater/sensor could arise and strongly affect the final measurement results. Absence of knowledge of this thermal contact resistance imposes significant uncertainties on the measured thermal conductivity. In addition, most of the experiments require a large-size sample in order to acquire sensible signals, in which case it is considerably difficult to preclude nanowires/tubes from touching each other. Hence the heat conduction occurring inside does

^{a)}Author to whom correspondence should be addressed; electronic mail: xwang3@unl.edu

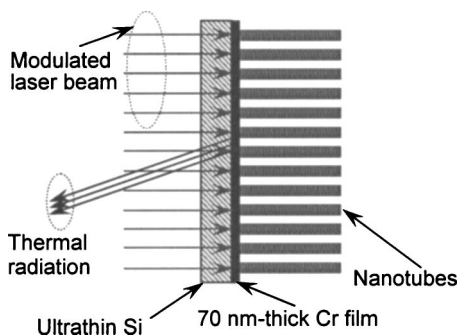


FIG. 1. Schematic of the experimental principles.

not follow the axial direction exclusively and the measured thermal conductivity is an average value reflecting the heat conduction in multidirection.

In this work, a photothermal experimental technique is developed to characterize the thermal conductivity of highly aligned multiwall CNTs. Due to the special design of the sample and the experimental technique, we are able to distinguish the thermal conductivity of CNTs and the thermal contact resistance between CNTs and the substrate. The experimental principles and details are presented in Sec. II while the experimental results are discussed in Sec. III.

II. DETAILS OF EXPERIMENT

In this section, first we present the experimental principles of the photothermal technique. Then we describe the experimental setup and how the experiment is conducted.

A. Experimental principles

Figure 1 shows the principles of the experiment. The sample used in our experiment embodies highly aligned CNTs perpendicularly grown on a 70 nm-thick Cr film that is coated on an ultrathin (14- μm -thick) Si wafer. A modulated laser beam is used to irradiate the backside of the silicon wafer. Ultrathin Si is chosen as the substrate because it has weak absorption of the infrared laser beam ($\lambda=1064$ nm) in our experiment and is transparent to the thermal radiation from the Cr surface. As a result, the laser beam induces direct heating of the Cr film, leading to a periodic temperature variation at the Cr surface. The heat conduction along CNTs strongly affects this temperature variation, which is sensed by measuring the surface thermal radiation. The phase shift of the thermal radiation relative to the laser beam is measured and used to determine the thermophysical properties of the sample. The phase shift of the thermal radiation is measured over a large frequency range. Trial values of unknown properties are used to compute the theoretical phase shift at each experimental frequency. The trial values giving the best fit (least square) of the experimental results are taken as the properties' value. In the experiment, the heating spot (the size of the focal point of the laser beam) is about 0.7 mm \times 1.4 mm. The modulation frequency of the laser beam is between 2 and 70 kHz. Within this frequency range, the thermal diffusion depth within one heating period in the lateral direction of the sample is much smaller than the heating spot.

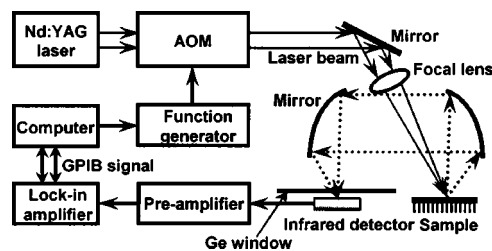


FIG. 2. Schematic of the experimental setup for characterizing the thermal transport in CNTs.

As a result, the thermal transport induced by laser heating can be treated one-dimensionally along the thickness direction of the sample.

B. Experimental setup

Figure 2 shows how the experiment is arranged and operated. A continuous Nd:yttrium–aluminum–garnet laser beam ($\lambda=1064$ nm) is modulated by an acousto-optic modulator (AOM) and then is focused on the CNT sample. The AOM is triggered to modulate the laser beam to be periodical square waves with the on/off time equal in each period. Different laser powers will heat the sample to different temperatures, which may affect the thermophysical properties of the samples. In our experiment, a laser beam of 200 mW (after modulation) is used, which assures sufficiently high thermal radiation signal from the Cr surface while keeping the sample temperature increase moderate to preclude large change of the thermophysical and optical properties of the sample. The laser beam has a Gaussian distribution in space. In the experiment, the spot of the laser beam on the sample is about $\sim 0.7 \times 1.4$ mm² (the beam is not perpendicular to the sample surface), which is much larger than the thermal diffusion depth in the lateral direction of the sample. As a result, the Gaussian distribution will have negligible effect on the measured phase shift. The thermal radiation from the Cr film (refer to Fig. 1) passes through the thin silicon wafer and is directed to an infrared detector. A Ge window is placed in front of the infrared detector to filter out the reflected laser beam and allows only the thermal radiation to pass. The signal from the infrared detector is preamplified and then is measured by a lock-in amplifier. The experiment is controlled by a PC for automatic data acquisition.

We are interested in measuring the phase shift (time delay) between the thermal radiation and the modulated laser beam, but the measurement will inevitably include a time delay induced by the system. This time delay is calibrated by measuring the reflected laser beam from the sample. In this calibration, the Ge window is removed. The signal measured by the infrared director consists of both the reflected laser beam and the thermal radiation. Our experiment indicates that the reflected laser beam is much stronger ($\sim 10^3$ times) than the thermal radiation, which ensures that the measured phase shift (ϕ_{cal}) in calibration is for the reflected laser beam. The phase shift of the reflected laser beam is induced by the system exclusively since reflection does not induce

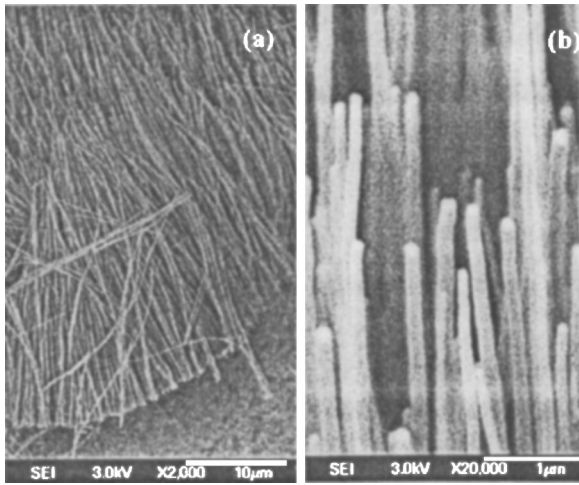


FIG. 3. Pictures of the CNT sample taken under a SEM. (a) Overall picture of CNTs on the substrate, and (b) top area of CNTs to show their high-degree alignment and size

time delay. The real phase shift of the thermal radiation is $\phi_{\text{mea}} - \phi_{\text{cal}}$, where ϕ_{mea} is the raw data of the measured phase shift for thermal radiation.

The phase shift of the thermal radiation is measured in a frequency (f) range of 2–100 kHz. At high frequencies, the thermal radiation signal is too weak in comparison with the noise. Therefore, in data reduction, only the data points between 2 and 70 kHz are used. This frequency range ensures that during the period of laser heating, the thermal penetration depth in the lateral direction of the sample is much smaller than the spot size of heating ($\sim 0.7 \times 1.4 \text{ mm}^2$). As a result, we only need to consider the one-dimensional heat conduction in the thickness direction of the sample. Trial values of unknown thermophysical properties of the sample will be used to calculate the theoretical phase shift. The trial values, which give the best fit (least square) of the experimental results, will be taken as the properties of the sample.

III. RESULTS AND DISCUSSION

The sample used in our experiment is obtained from Nano-lab, Inc. The CNTs were fabricated using plasma-enhanced hot filament chemical vapor deposition. Details of the fabrication procedure are discussed in work by Ren's group.^{17–19} Figure 3 shows pictures of the sample taken under a scanning electron microscope (SEM). In Fig. 3(a) it is observed that the CNTs are highly aligned. Carbon nanotubes look tilted in Fig. 3(a) because they were stripped off the substrate for sample preparation in order to be observed under the SEM. Figure 3(b) indicates that the diameter of CNTs is around 100–200 nm. The length of the CNT array is about 20 μm based on the observation under the SEM. As mentioned in the experimental principles (Sec. II A), a 70-nm-thick Cr coating is deposited between the end of CNTs and the Si substrate.

A. Experimental results

Figure 4 presents the measured phase shift for the reflected laser beam in calibration. Without instrument time

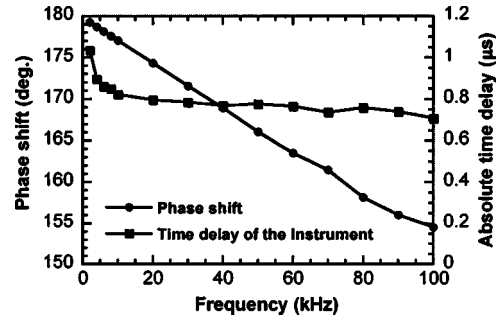


FIG. 4. Measured phase shift of the reflected laser beam and absolute time delay induced by the instrument.

delay, this phase shift would be 180° because the zeroth order of the deflected laser beam from the AOM is used to irradiate the sample surface. From the measured phase shift, the absolute time delay induced by the system is calculated as $(180 - \phi_{\text{cal}})/360/f$ where f is the modulation frequency. In Fig. 4 it is evident that the time delay induced by the system is about 700 ns ($1 \text{ ns} = 10^{-9} \text{ s}$). Figure 5 displays the absolute phase shift of the thermal radiation signal from the Cr surface, as well as the fitting results. For experimental result fitting, the physical model developed by Hu and Wang^{20,21} is employed. In work by Hu and Wang,^{20,21} the laser beam was used to irradiate the sample surface. The air pressure variation in the region adjacent to the sample surface was measured and used to determine the thermophysical properties of samples. In this work, the laser beam is used to irradiate an interface inside the sample. Thermal radiation from the inside interface is measured and used to determine the thermophysical properties of a specific layer. In this work, the sample consists of different layers, including the air at the top of the CNT array, the CNT array, Cr film, Si substrate, and the air below the Si substrate. Volumetric absorption of the laser beam in the Cr coating and the thermal contact resistance at the CNT/Cr and Cr/Si interfaces are considered. It is evident that the fitting result and the experimental data agree well each other. Since it is hard to directly tell the difference between the fitting result and the experimental data in the figure, we also plot the difference between them (diamond in the figure). It is observed that this phase shift difference is around or less than 0.2° , which is consistent with the experimental uncertainty observed in our experiment. Based on phase shift fitting, the effective density (ρ_{eff})

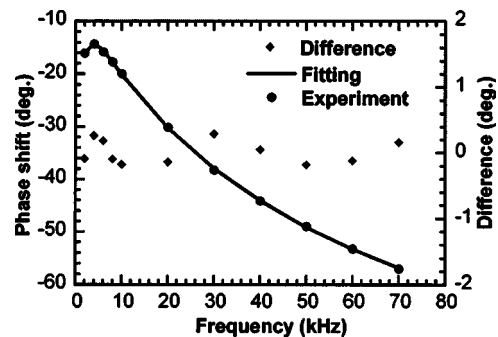


FIG. 5. Data fitting of the absolute phase shift of the thermal radiation from the sample surface.

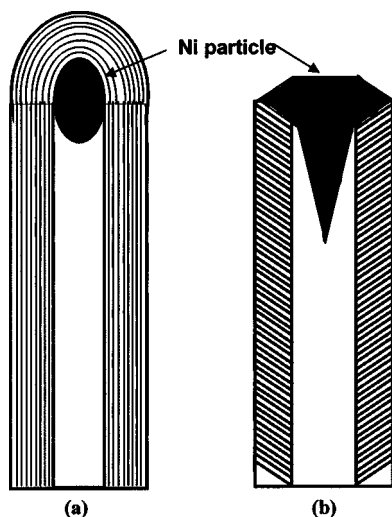


FIG. 6. (a) Multiwall carbon nanotubes with structures preferable for thermal transport in the axial direction, and (b) schematic of the structure of CNTs characterized in this work.

and effective thermal conductivity (k_{eff}) of the CNT array are determined to be 11.72 kg/m^3 and 0.145 W/m K , respectively. Since the structure of CNTs is close to that of graphite, we use the density of graphite (ρ) 2210 kg/m^3 as the density of CNTs to calculate the absolute thermal conductivity (k) of individual CNTs as $k = \rho / \rho_{\text{eff}} \times k_{\text{eff}} = 27.3 \text{ W/m K}$. This relationship is physically reasonable because the thermal transport is only along the axial direction of CNTs in our experiment. Based on data fitting, we also determine that the thermal contact resistance at the CNT/Cr interface is less than $3 \times 10^{-8} \text{ K m}^2/\text{W}$, in which the effects of the space between CNTs and within CNTs are already excluded based on the effective density of the CNT array. The exact value of this thermal contact resistance is too small to be determined by our current photothermal technique. In the experiment, based on phase shift data fitting, the thermal contact resistance between the Cr coating and the Si substrate is determined to be $1.643 \times 10^{-5} \text{ K m}^2/\text{W}$. During sample preparation for making CNTs, such as coating the Si substrate with Cr, the Si substrate is too fragile ($14 \mu\text{m}$ -thick) to be cleaned thoroughly before coating Cr. Therefore, the contamination on the Si surface could give rise to this large thermal contact resistance. After the Cr coating is made, the sample is immediately prepared for CNT synthesis. Therefore, the thermal contact resistance between CNTs and the Cr coating is relatively small.

B. Experimental result interpretation

The above measured thermal conductivity (27.3 W/m K) of multiwall CNTs along the axial direction is much smaller than published theoretical predictions ($1600\text{--}6600 \text{ W/m K}$) for SWCNTs. One reason for this difference is the special structure of the measured CNTs in our work. Figure 6 shows two different structures of CNTs. Structure (a) is the one used in theoretical prediction of the thermal conductivity of CNTs along the axial direction, in which the atomic layer in the tube wall is along the axial

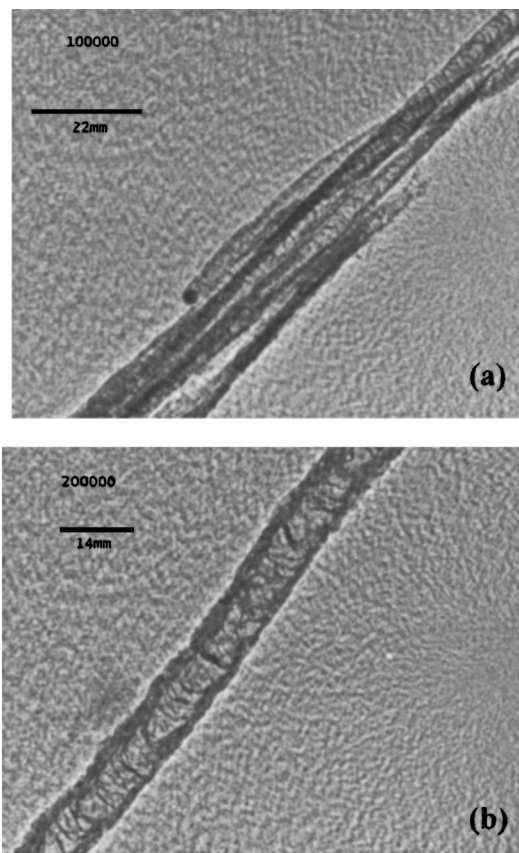


FIG. 7. Carbon nanotubes observed under TEM. The scale bar represents 220 nm in Fig. 7(a) and 70 nm in Fig. 7(b).

direction. The published high thermal conductivity of SWCNTs is along the atomic layer direction. Structure (b) is for the CNTs measured in our work, which were grown from a thin Ni film coated on a Cr film. In the experiment for growing CNTs, the Ni film cracked and shrank to become Ni nanoparticles. These Ni particles left the Cr surface and stayed at the tip of CNTs to promote tip growth. Therefore, in fitting of the experimental data, the Ni film is not considered. Due to the special structure of the Ni particle, the atomic layer of the CNT wall is not along the axial direction of the tube, but tilted with respect to the tube axis.²² As a result, the measured thermal conductivity in the axial direction is across the atomic layer, explaining why the measured thermal conductivity is much lower than the theoretical predictions. The other reason for the measured low thermal conductivity of CNTs is their poor structural quality. Figure 7 displays some of the measured CNTs observed under a transmission electron microscope (TEM). For sample observation under the TEM, we first scratch a small amount of CNTs off the substrate and disperse them into methanol. Then the mesh used for the TEM is dipped into the solution to deposit CNTs on the mesh for observation under the TEM. The scale bar in the picture represents 220 nm in Fig. 7(a) and 70 nm in Fig. 7(b). It is evident that the thickness of the CNT wall is not uniform and there are a large number of defects in the tube. These defects strongly increase phonon scattering and reduce the thermal conductivity. At present, we are doing experiments to study the thermal transport in high-quality CNTs using the experimental setup described in this article.

IV. CONCLUSION

In this work, a photothermal experiment was designed and conducted to characterize the thermal transport along the axial direction of multiwall CNTs. Due to the unique thermal depth profiling of the technique, we characterized the thermal contact resistance between CNTs and the substrate. The measured value demonstrated a sound thermal contact between them. The experimental result revealed a low thermal conductivity of CNTs along the axial direction. This low thermal conductivity probably was due to the unique structure of the CNTs in our work, which indicated that the thermal transport in the axial direction was across the atomic layer of carbon atoms. In addition, our TEM observation of the CNTs revealed poor structural qualities, which can strongly enhance phonon scattering and reduce the thermal conductivity.

ACKNOWLEDGMENTS

Support for this work from the National Science Foundation (CTS: 0210051) and the University of Nebraska-Lincoln through the Layman Award is greatly acknowledged. The authors are grateful for the support of this work from the College of Engineering and Technology and the Department of Mechanical Engineering at UNL through the faculty start-up fund.

¹M. S. Dresselhaus and P. C. Eklund, *Adv. Phys.* **49**, 705 (2000).

²S. Berber, Y. Kwon, and D. Tománek, *Phys. Rev. Lett.* **84**, 4613 (2000).

³M. A. Osman and D. Srivastava, *Nanotechnology* **12**, 21 (2001).

⁴J. Che, T. Çağın, and W. A. Goddard III, *Nanotechnology* **11**, 65 (2000).

⁵S. Maruyama, *Microscale Thermophys. Eng.* **7**, 41 (2003).

⁶J. Hone, M. Whitney, C. Piskoti, and A. Zettl, *Phys. Rev. B* **59**, R2514 (1999).

⁷J. Hone, M. C. Llaguno, N. M. Nemes, A. T. Johnson, J. E. Fischer, D. A. Walters, M. J. Casavant, J. Schmidt, and R. E. Smalley, *Appl. Phys. Lett.* **77**, 666 (2000).

⁸J. Hone, M. C. Llaguno, M. J. Biercuk, A. T. Johnson, B. Batlogg, Z. Benes, and J. E. Fischer, *Appl. Phys. A: Mater. Sci. Process.* **74**, 339 (2002).

⁹J. Vavro, M. C. Llaguno, B. C. Satishkumar, D. E. Luzzi, and J. E. Fischer, *Appl. Phys. Lett.* **80**, 1450 (2002).

¹⁰L. Shi, D. Li, C. Yu, W. Jang, D. Kim, Z. Yao, P. Kim, and A. Majumdar, *ASME J. Heat Transfer* **125**, 881 (2003).

¹¹W. Yi, L. Lu, D. Zhang, Z. Pan, and S. Xie, *Phys. Rev. B* **59**, R9015 (1999).

¹²S. Xie, W. Li, Z. Pan, B. Chang, and L. Sun, *J. Phys. Chem. Solids* **61**, 1153 (2000).

¹³L. Lu, W. Yi, and D. L. Zhang, *Rev. Sci. Instrum.* **72**, 2996 (2001).

¹⁴T. Borca-Tasciuc, C. L. Hapenciuc, B. Wei, R. Vajtai, and P. M. Ajayan, *ASME International Mechanical Engineering Congress and Expositions*, Nov. 17–22, 2002, New Orleans, LA, 2002, paper No. 39576.

¹⁵D. J. Yang, Q. Zhang, G. Chen, S. F. Yoon, J. Ahn, S. G. Wang, Q. Zhou, Q. Wang, and J. Li, *Phys. Rev. B* **66**, 165440 (2002).

¹⁶P. Kim, L. Shi, A. Majumdar, and P. L. McEuen, *Phys. Rev. Lett.* **21**, 215502 (2001).

¹⁷Z. P. Huang, J. W. Xu, Z. F. Ren, J. H. Wang, M. P. Siegal, and P. N. Provencio, *Appl. Phys. Lett.* **73**, 3845 (1998).

¹⁸Z. F. Ren, Z. P. Huang, J. W. Xu, J. H. Wang, P. Bush, M. P. Siegal, and P. N. Provencio, *Science* **282**, 1105 (1998).

¹⁹Z. F. Ren, Z. P. Huang, D. Z. Wang, J. G. Wen, J. W. Xu, J. H. Wang, L. E. Calvet, J. Chen, J. F. Klemic, and M. A. Reed, *Appl. Phys. Lett.* **75**, 1086 (1999).

²⁰H. Hu, X. Wang, and X. Xu, *J. Appl. Phys.* **86**, 3953 (1999).

²¹X. Wang, H. Hu, and X. Xu, *ASME J. Heat Transfer* **123**, 138 (2001).

²²J. G. Wen, Z. P. Huang, D. Z. Wang, J. H. Chen, S. X. Yang, Z. F. Ren, J. H. Wang, L. E. Calvet, J. Chen, J. F. Klemic, and M. A. Reed, *J. Mater. Res.* **16**, 3246 (2001).